Molecular Immunology 120 (2020) 1–12

Contents lists available at ScienceDirect

Molecular Immunology

journal homepage: www.elsevier.com/locate/molimm

The allergen Mus m 1.0102: Cysteine residues and molecular allergology

Elena Ferrari[a], Romina Corsini[a,1], Samuele E. Burastero[b], Fabio Tanfani[c], Alberto Spisni[a,*]

[a] Dept. Medicine and Surgery, University of Parma, via Gramsci 14, 43126, Parma, Italy
[b] Div. Immunology, IRCCS San Raffaele, Via Olgettina 60, 20132, Milano, Italy
[c] Dept. Life and Environmental Sciences, Marche Polytechnic University, via Brecce Bianche, 60131, Ancona, Italy

ARTICLE INFO

Keywords:
Mus m 1.0102 allergen
Molecular allergology
Cysteine
Thermal stability
Protein aggregation
Unfolding reversibility

ABSTRACT

Mus m 1.0102 is a member of the mouse Major Urinary Protein family, belonging to the Lipocalins superfamily. Major Urinary Proteins (MUPs) are characterized by highly conserved structural motifs. These include a disulphide bond, involved in protein oxidative folding and protein structure stabilization, and a free cysteine residue, substituted by serine only in the pheromonal protein Darcin (MUP20). The free cysteine is recognized as responsible for the onset of inter- or intramolecular thiol/disulphide exchange, an event that favours protein aggregation.

Here we show that the substitution of selected cysteine residues modulates Mus m 1.0102 protein folding, fold stability and unfolding reversibility, while maintaining its allergenic potency.

Recombinant allergens used for immunotherapy or employed in allergy diagnostic kits require, as essential features, conformational stability, sample homogeneity and proper immunogenicity. In this perspective, recombinant Mus m 1.0102 might appear reasonably adequate as lead molecule because of its allergenic potential and thermal stability. However, its modest resistance to aggregation renders the protein unsuitable for pharmacological preparations. Point mutation is considered a winning strategy.

We report that, among the tested mutants, C138A mutant acquires a structure more resistant to thermal stress and less prone to aggregation, two events that act positively on the protein shelf life. Those features make that MUP variant an attractive lead molecule for the development of a diagnostic kit and/or a vaccine.

1. Introduction

The mouse Major Urinary Protein complex (MUPs) comprises a variety of isoforms with high similarity (Logan et al., 2008) characterized by a number of conserved structural motifs, among them one disulphide bond and a free cysteine residue recognized to be responsible for the onset of inter- or intramolecular thiol/disulphide exchange, an event that favours protein aggregation. The free cysteine is substituted by serine only in the pheromonal protein Darcin (MUP 20).

MUPs are mainly produced in the liver, excreted *via* the urine and deposited on the ground where they act as chemical signals allowing communication among rodents (Roberts et al., 2018; Tirindelli et al., 2009; Hurst et al., 2001).

Mice urine deposition, however, has a detrimental effect on humans. In fact, MUP proteins are also identified as the major mouse allergen Mus m 1, a primary cause of allergic sensitization and allergic respiratory disease in sensitized individuals (Jeal and Jones, 2010; Matsui, 2009; Bush and Stave, 2003). Noteworthy, airborne mouse allergen concentration measured in many US inner-city homes has proved to be similar to the values found in animal facilities, where the levels are high enough to trigger asthma symptoms (Matsui et al., 2005; Zahradnik and Raulf, 2014).

In the last two decades, molecular investigations on recombinant MUPs led to relevant outcomes and challenges. Recombinant MUPs were expressed and purified (Ferrari et al., 1997; Timm et al., 2001), the structure of some of them was resolved at high-resolution both by NMR and X-ray crystallography (Timm et al., 2001; Lücke et al., 1999; Phelan et al., 2014; Böcskei et al., 1992; Kuser et al., 2001) and their ligand binding properties were extensively characterized (Ferrari et al., 1997; Timm et al., 2001; Phelan et al., 2014; Böcskei et al., 1992; Kuser et al., 2001; Ricatti et al., 2019; Pertinhez et al., 2009; Sharrow et al., 2005; Sartor et al., 2001).

The new concept in allergy diagnosis, namely the *Component Resolved Diagnosis* (CRD), has made possible to map the allergen

* Corresponding author at: Dept. Medicine and Surgery, University of Parma, via Gramsci 14, 43126, Parma, Italy.
E-mail addresses: elena.ferrari@unipr.it (E. Ferrari), romina.corsini@ausl.re.it (R. Corsini), burastero.samuele@hsr.it (S.E. Burastero), f.tanfani@univpm.it (F. Tanfani), alberto.spisni@unipr.it (A. Spisni).
[1] Present address: Arcispedale Santa Maria Nuova, Reggio Emilia, Italy.

https://doi.org/10.1016/j.molimm.2020.01.022
Received 26 October 2019; Received in revised form 23 January 2020; Accepted 29 January 2020

sensitization profile of a patient at a molecular level, provided that each allergen is available in purified form (Matricardi et al., 2016; Canonica et al., 2013; Sastre, 2010). To address this demand, when dealing with protein allergens, their recombinant form represent a good option given that the recombinant protein: 1) is closely related to the native protein in terms of structural and physicochemical properties, 2) it exhibits comparable IgE reactivity and 3) meets the quality standards of manufacturing: product homogeneity and stability; batch to batch consistency.

Given these features, molecular diagnostics allows to identify the triggering allergenic molecule, making the patients eligible for Specific Immunotherapy (SIT): the only allergen-specific form of treatment that, through gradual allergen administration, induces tolerance and reduces reactivity to the allergen, preventing the progression toward severe allergy manifestations (Jutel et al., 2015). Interestingly, allergy vaccines based on recombinant allergens overcome many of the problems associated with the difficult standardization and management of allergenic extracts prescriptions (Wintersand et al., 2019; Tscheppe and Breiteneder, 2017; Nandy et al., 2015; Cantillo and Puerta, 2013).

Knowing that an environmental allergen detection system, specific for MUPs and based on polyclonal antibodies raised against recombinant MUP10 [Ferrari et al., 2004, INDOORS Biotechnologies ltd, Cardiff, UK], is already available on the market, we have good expectation for the use of this recombinant protein in clinical practice.

To meet this challenge, we produced and tested a number of mutants of the recombinant Mus m 1.0102 (MUP10) (Ferrari et al., 1997, 2012; Ferrari et al., 2016), focusing on enhancing its structural stability while preserving its immunogenicity: the target benchmarks for a biotechnological product (Nandy et al., 2015).

In a previous work, studying its mutant MM-C138S we proved that the free cysteine, Cys138, whose side chain is packed in the hydrophobic interface between the β-barrel and the α-helix (Fig. 1), is responsible for inter- or intra-molecular thiol/disulphide exchange, thus promoting protein aggregation (Ferrari et al., 2016).

In this work, aiming to extend the protein functional lifetime and to preserve its immunogenic activity (Xia et al., 2015), we studied the mutants: a) MM-C138A where the small hydrophobic Ala has been preferred to the polar and H-bond forming Ser (Ferrari et al., 2016), b) MM-C157A, where the native disulphide bond is obliterated and c) MM-C138,157A, a double mutant where the possibility to form intra-molecular disulphide bridges is ruled out.

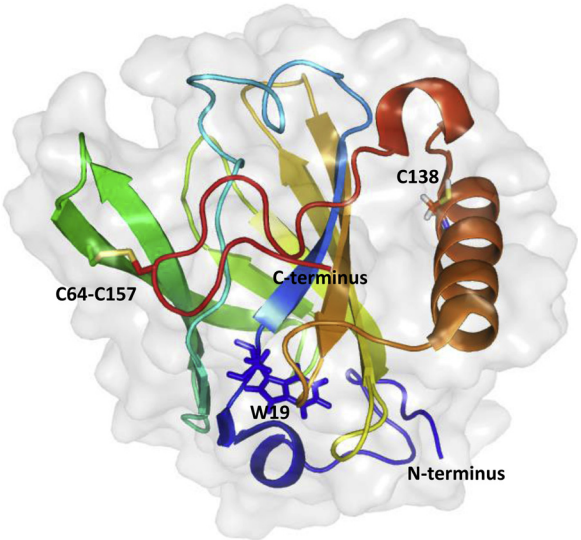

Fig. 1. NMR structure of Mus m 1.0102 (PDB: 1DF3, model 1) in cartoon representation. Residue C138 side chain and the disulphide bridge C64-C157 are evidenced in sticks to highlight the selected mutagenesis sites used to produce the single mutants MM-C138A and MM-C157A, which abolish the free buried thiol and the native disulphide bond, respectively, and the double mutant MM-C138,157A that excludes any intra-molecular disulphide bridge. The single Trp (W19) side chain is evidenced in sticks. The software *PyMOL Molecular Graphics System, Schrödinger* was used to generate this image.

2. Materials and methods

2.1. Protein expression, purification and western blot analysis

Recombinant Mus m 1.0102 was expressed in *Pichia pastoris* and purified as described (Ferrari et al., 2016). Synthetic genes (Eurofins Genomics), encoding either MM-C138A, or MM-C157A or MM-C138,157A protein and all including an N-terminal Enterokinase cleavage site, were cloned into pGEX expression vector to produce GST-fused proteins; the constructs were sequenced to confirm the DNA sequence of each insert. Fusion proteins expression was induced by adding 1 mM isopropil-β-d-1-thiogalactopyranoside (Sigma-Aldrich) to *E. coli* Rosetta (DE3) pLysS (Novagen) transformant cells and culturing them for 4 h. Culture cells were lysed with BugBuster Protein Extraction Reagent plus Benzonase Nuclease (Novagen), according to the manufacturer's protocol, obtaining a fusion protein yield of about 10 mg per litre of bacterial culture. The GST-tagged proteins in the soluble fraction were affinity purified by means of GST Bulk Kit (GE Healthcare Life Sciences) and cleaved by Enterokinase protease (Novagen), according to the manufacturer's protocol. Protein concentrations were determined spectrophotometrically, using an extinction coefficient at 278 nm obtained by theoretical calculation (Pace et al., 1995).

After SDS-PAGE electrophoresis (12 % acrylamide), equal amounts of the cloned proteins were electro-blotted onto Immobilon-P Membrane, PVDF (Merck Millipore) and incubated over-night at 4 °C with rabbit anti-MUP polyclonal antibody (MUP FL180 antibody, Santa Cruz Biotechnology, 1:200 dilution). Detection was performed with HRP-conjugated anti-rabbit IgG antibodies (Sigma-Aldrich, 1:200,000 dilution) by enhanced chemiluminescence autoradiography (Chemiluminescence Western Blotting Substrate POD, Roche).

2.2. Circular dichroism and fluorescence spectroscopy

2.2.1. Circular dichroism spectroscopy

CD spectra were acquired with a JASCO J-715 spectropolarimeter, equipped with a Peltier-controlled cuvette holder. Spectra were collected at scan speed of 20 nm/min and with a response time of 1 s. Each spectrum was the average of three scans to achieve appropriate signal-to-noise ratios. Far-UV CD and near-UV CD spectra were collected at protein concentrations of 4 μM and 100 μM with a 1 mm and 0.2 cm path length cell, respectively. Acquired data were expressed as mean molar residue ellipticity, [θ] deg cm^2 $dmol^{-1}$.

2.2.2. Fluorescence spectroscopy

Measurements were performed on a JASCO FP-6200 spectrofluorometer, equipped with a Peltier-controlled cuvette holder. Tryptophan fluorescence was monitored by exciting at 295 nm, using a bandwidth of 5 nm on both monochromators. The emission spectra were recorded over a 310–550 nm wavelength range, with a 1 cm path length cell and using a sample concentration of 2 μM.

2.2.3. Thermal unfolding/refolding

CD and fluorescence unfolding measurements were carried out in 10 mM potassium phosphate buffer pH 7.2.

The CD signal at 202 nm was recorded as a function of temperature in the range 25 − 90 °C, at intervals of 0.2 °C and heating rate of 1 °C min^{-1}.

The wavelength of the fluorescence emission maximum (λ_{max}) has been recorded as a function of temperature in the range 25–90 °C at 5 °C intervals, with equilibration time of 5 min for each step. CD refolding measurements were carried out by cooling back towards the starting

temperature (with the same ramp rate and acquiring data at the same wavelength).

As for the fluorescence refolding measurements, samples were gradually cooled back to 25 °C, equilibrated at 25 °C for 1 h and subsequently the whole fluorescence spectrum was recorded.

2.3. Fourier-transform infrared spectroscopy (FTIR)

Infrared spectroscopy is a powerful tool for the study of the secondary structure of proteins in solution. However, IR spectra of proteins in H_2O (or ^1H_2O) suffer of the strong absorption of water occurring in the same spectral region useful for the analysis of protein secondary structure (amide I band, $1700-1600\ cm^{-1}$). Furthermore, discrimination of α-helices and random coils in spectra obtained in water is not possible, since these two structures give rise to largely overlapping bands. These drawbacks can be avoided by preparing protein samples in heavy water, (where hydrogen, ^1H, is substituted by deuterium, ^2H or D: deuterium oxide, ^2H_2O or D_2O) since this medium shows only a small absorption in the $1700-1600\ cm^{-1}$ spectral region and allows the α-helices and random coils bands to be easily distinguished.

2.3.1. Sample preparation

Mus m 1.0102 and the MM-C157A mutant were analysed in buffers prepared in ^2H_2O. Heavy water (99.9 % ^2H), sodium deuteroxyde (NaO^2H), deuterium chloride (^2HCl), and Tris(2-carboxyethyl)phosphine (TCEP) were from Sigma Aldrich. The buffers used for protein analysis were 25 mM Hepes/NaO^2H p^2H 7.2 (buffer A) or 25 mM Piperazine/^2HCl, 5 mM TCEP p^2H 5.5 (buffer B). TCEP was used to reduce the disulphide bridge (Burns et al., 1991). The p^2H value was measured with a standard pH electrode, and the pH value was corrected according to the formula p^2H = pH meter reading + 0.4 (Salomaa et al., 1964). Sample solutions, containing about 1.3 mg of protein, were centrifuged in 10 K Amicon ultra 0.5 micro-concentrator (Millipore Ireland Ltd, Cork, IRL) at 10,000 x g, at 4 °C, until the final volume of approximately 30 µL. Then, after the addition of 200 µl of either buffer A or B, the solution was re-concentrated to the same final volume; this procedure was repeated five times in order to achieve a complete buffer exchange. The final concentration of the protein solution for infrared analysis was approximately 30 mg/mL.

2.3.2. Infrared spectra acquisition and processing

Concentrated protein samples were injected into a thermostated Graseby Specac 20500 cell Graseby-Specac Ltd, Orpington, Kent, UK fitted with CaF_2 windows and a 25 µm mylar spacer. FT-IR spectra were recorded at 20 − 90 °C by means of a Perkin-Elmer 1760-x Fourier transform infrared spectrometer using a deuterated triglycine sulphate detector and a normal Beer-Norton apodization function.

At least 24 h before and during data acquisition, the spectrometer was continuously purged with dry air at a dew point of −70 °C by using a Parker Balston 75-62 FT-IR air dryer (Balston AGS, Haverhill, MA). To obtain spectra at different temperatures an external bath circulator (HAAKE F3) was employed. In thermal denaturation experiments, spectra were collected at 5 °C intervals in the 20 − 90 °C temperature range with equilibration time of 5 min for each step. The actual temperature in the cell was controlled by a thermocouple placed directly onto the CaF_2 windows. Spectra of buffers and samples were acquired at $2\ cm^{-1}$ resolution, under the same scanning and temperature conditions. Typically, 256 scans were averaged for each sample recorded at 20 °C, whilst 32 scans were averaged for samples recorded in the 25 − 90 °C temperature range. Subtraction of the small absorption of heavy water in the amide I' region (amide I band in water) consisted in the removal of ^2H_2O bending absorption close to $1220\ cm^{-1}$ (Ausili et al., 2005). After buff ;er subtraction, all the absorbance spectra were normalized to the same amide I' band area in order to neutralize small diff ;erences in protein concentration among the concentrated samples.

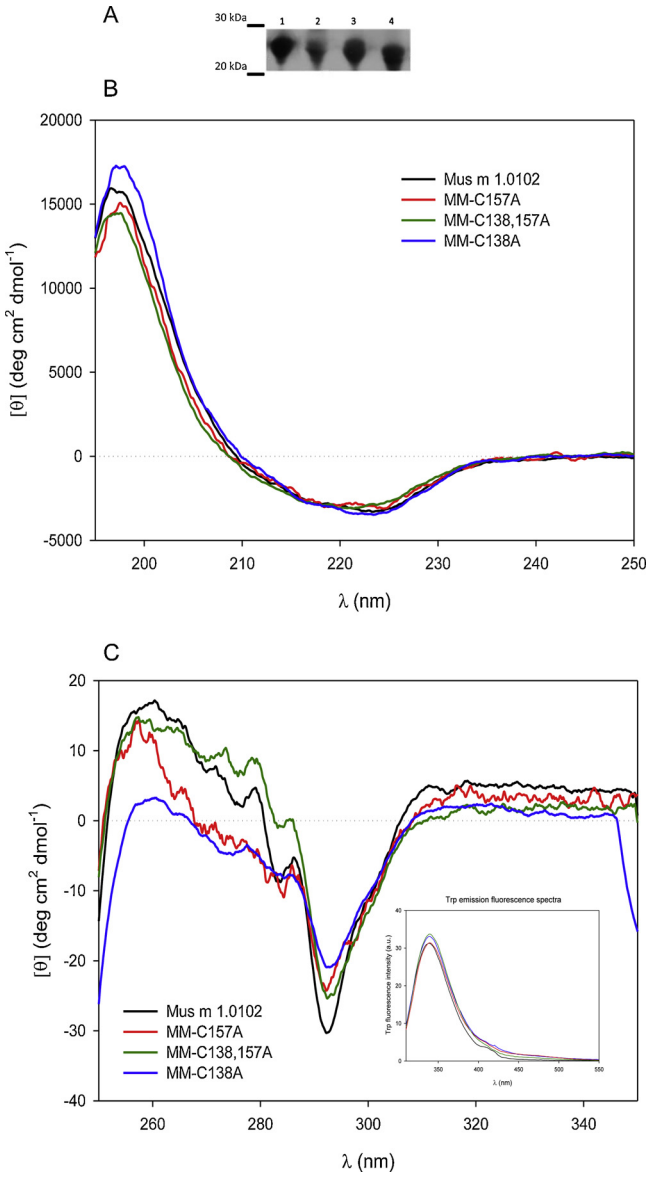

Fig. 2. Protein identification and conformational characterization. A. Western blot: Mus m 1.0102 (lane 1), MM-C138A (lane 2), MM-C157A (lane 3) and MM-C138,157A (lane 4) samples were detected and properly identified by means of a rabbit anti-Mus m 1 polyclonal antibody. B. Far-UV CD spectra and C. Near-UV CD spectra. Inset panel C: Tryptophan emission spectra of Mus m1.0102 and its mutants. (For interpretation of the references to colour in this figure legend, the reader is referred to the web version of this article).

Table 1
Ligand binding and thermal unfolding parameters of Mus m 1.0102 and its mutants.

Optical Technique parameter	*Fluorescence Kd[a] (nM)*	*DLS Tm_{onset}[b] (°C)*	*CD Tm[c] (°C)*	*Fluorescence Tm[c] (°C)*
Mus m 1.0102	25.0 ± 1.5	62.5	76.3 ± 0.1	75.2 ± 0.5
MM-C138A	33.8 ± 6.4	70.0	76.7 ± 0.2	78.9 ± 1.3
MM-C157A	85.5 ± 13.7	52.5	67.3 ± 0.2	70.6 ± 2.8
MM-C138,157A	45.2 ± 4.0	55.0	62.9 ± 0.2	67.4 ± 1.5

[a] Dissociation constants (Kd ± SE) were calculated by titration experiments using N-Phenyl-1-naphthylamine fluorescent probe (Data in brief co-submitted article). [b]Temperatures associated to the onset of unfolding (Tm_{onset}) were obtained by DLS measurements (Data in brief co-submitted article). [c]Transition midpoints (Tm ± SE) derive from CD and Intrinsic Fluorescence spectroscopy data.

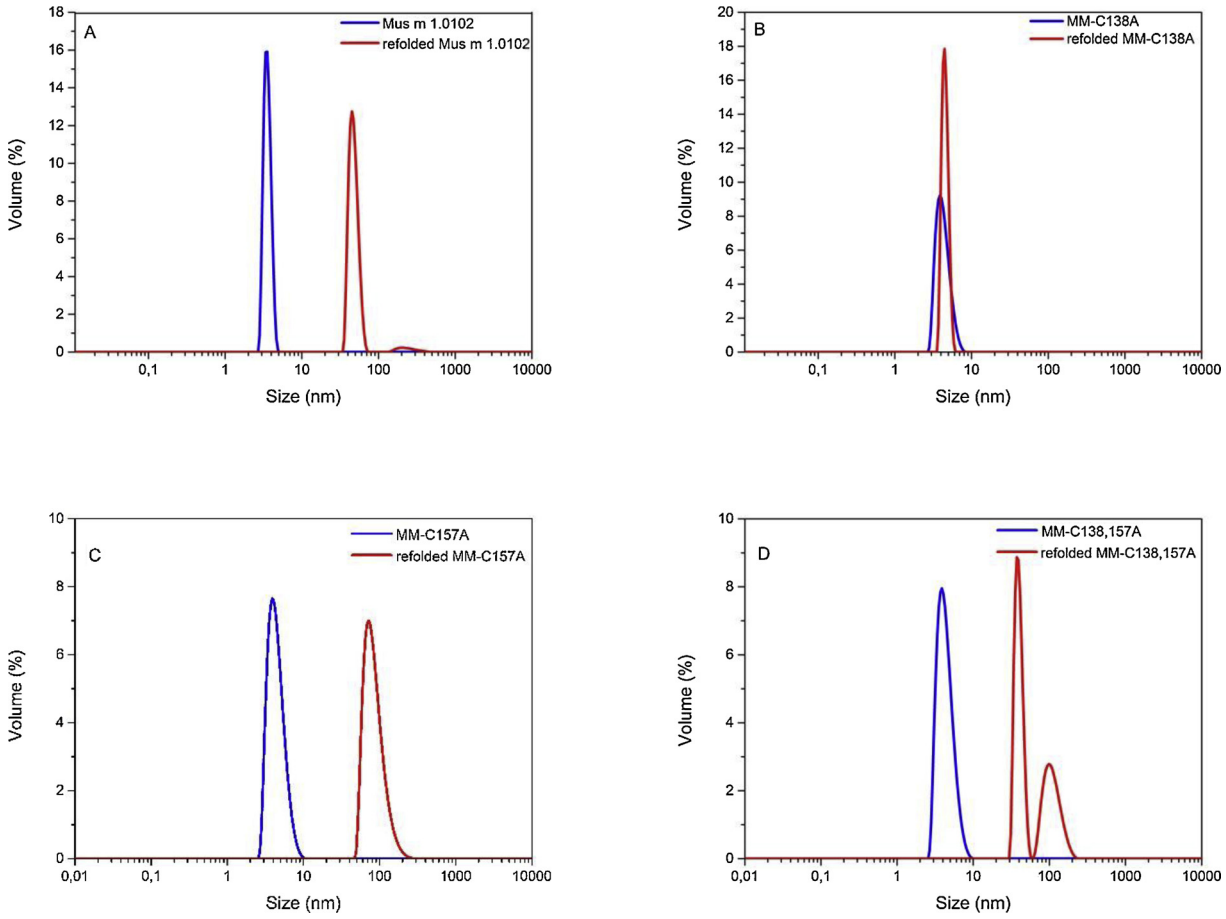

Fig. 3. Protein refolding monitored by DLS derived size distribution. Particle size distributions by volume (%) are expressed as a function of particle diameter (nm, in log scale) and were derived from the DLS intensity profiles of light scattered by solutions of Mus m 1.012 and its mutants (A–D panels). *Blue trace*: proteins in native conditions. *Red trace:* refolded proteins, at 25 °C, after the thermal denaturation. Sizes ranging around 4 nm are compatible with the monomeric protein hydrodynamic size; higher values are indicative of protein aggregates. (For interpretation of the references to colour in this figure legend, the reader is referred to the web version of this article).

Spectra were processed using the SPECTRUM software, Perkin-Elmer. Deconvoluted parameters were set with a gamma value of 2.3 and a smoothing length of 60. Second-derivative spectra were calculated over a 9 data-point range (9 cm^{-1}).

2.4. Dynamic light scattering (DLS)

DLS is based on the analysis of the temporal fluctuations of the light scattering intensity caused by macromolecules in solution and provides information on protein hydrodynamic radius, relying on the intensity-weighted distribution of the particle sizes in solution. For this set of experiments, recombinant proteins were dissolved in Tris-HCl 10 mM pH 7.2 at concentrations ranging from 45 to 240 μM and filtered (Anotop siringe filter 0.02 μm, Whatman) before use. Measurements were carried out using a Malvern Zetasizer μV instrument.

2.4.1. Molecular size distribution profiles

Light Intensity fluctuations were collected and analysed by Malvern algorithms to produce distributions of the hydrodynamic diameter of the molecules in solution. Molecular size distribution profiles of the proteins were compared in native and refolding conditions, following the heat treatment up to 80 °C (Data in brief co-submitted article) and a refolding time of 30 min at 25 °C. To probe sample homogeneity, the intensity-weighted distributions were converted to volume-weighted distributions, reflecting the relative proportion of multiple molecular sizes based on their volume (Stetefeld et al., 2016). The mean hydrodynamic diameter was used for peak comparison and distribution analysis.

3. Results

3.1. Epitopes reactivity and binding ability of Mus m 1.0102 and selected CYS mutants

3.1.1. Western blot

Purified recombinant Mus m 1.0102 and its mutants MM-C138A, MM-C157A, MM-C138,157A were detected and properly identified by means of western blot analysis using a rabbit anti-Mus m 1 polyclonal antibody (Fig. 2A). The ability of all proteins to bind to the rabbit anti-Mus m 1 polyclonal antibody indicate the correct exposure of the epitopes.

Based on these findings, protein samples were considered suitable for further functional and conformational characterization.

3.1.2. Ligand binding

To test the ligand binding ability of the mutants we performed direct titration experiments with N-Phenyl-1-naphthylamine (NPN), a fluorescent probe with high specificity for the hydrophobic pocket of Mus m 1.0102 (Pertinhez et al., 2009; Darwish et al., 2001). The experimental conditions and the fluorescence titration data are presented in the Data in brief co-submitted article. The dissociation constants (Kd) are reported in Table 1.

The results indicate that both the disulphide bridge and Cys138 residue influence the structural and dynamic organization of the

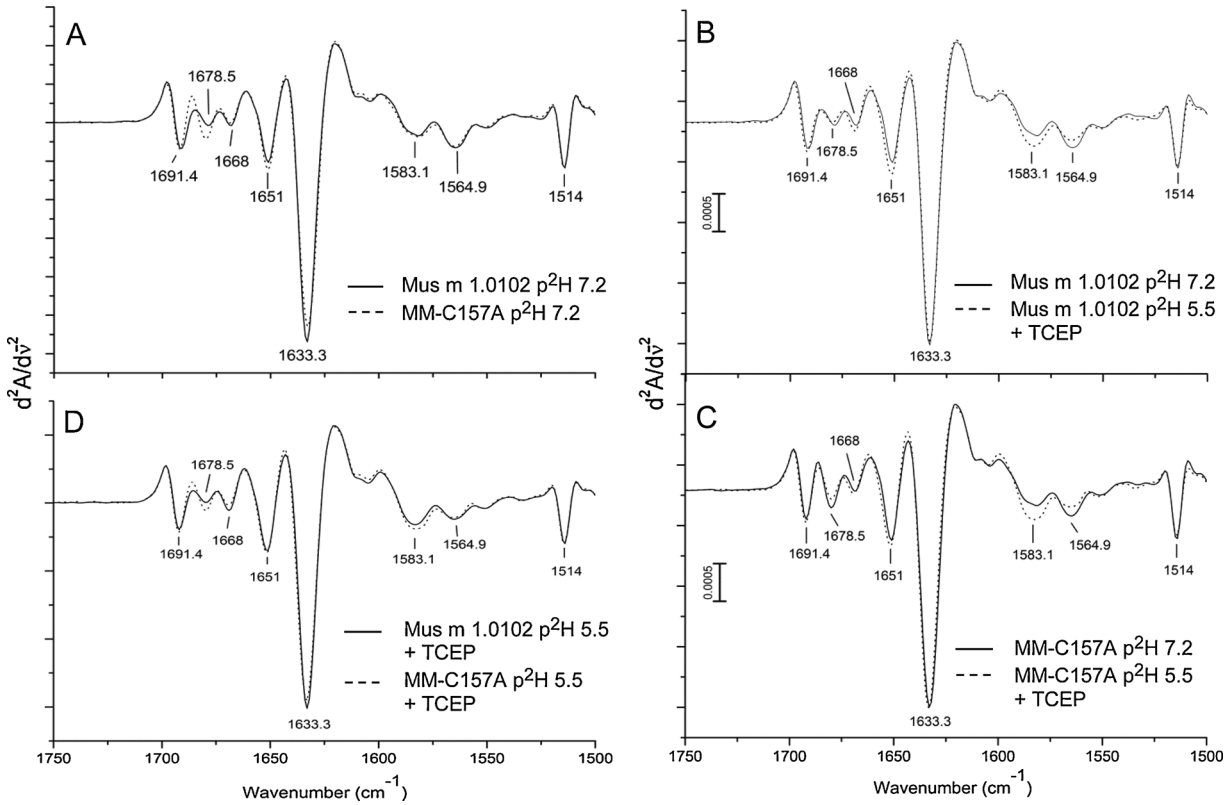

Fig. 4. FTIR second derivative spectra. Continuous and dashed lines refer, respectively, to: A, Mus m 1.0102 and MM-C157A at p^2H 7.2; B. Mus m 1.0102 at p^2H 7.2 and at p^2H 5.5 in the presence of TCEP; C. MM-C157A at p^2H 7.2 and at p^2H 5.5 in the presence of TCEP; D. Mus m 1.0102 and MM-C157A mutant at p^2H 5.5 in the presence of TCEP.

binding pocket. However, based on the standard errors associated to the mutants' Kd values, their binding curves appear less accurate in describing the protein binding behaviour as compared to the Mus m 1.0102 one.

3.2. Structural features of Mus m 1.0102 and its mutants in native conditions

3.2.1. Circular dichroism spectroscopy

The far-UV CD spectra of Mus m 1.0102 and its mutants exhibit a common profile consistent with a predominantly β-sheet architecture (Fig. 2B), suggesting the native secondary structure is preserved. However, differences are present in the profile of the near-UV CD spectra. Mus m 1.0102 and MM-C138,157A present detectable positive dichroic bands in the spectral region 260 − 285 nm. Instead, MM-C138A and MM-C157A barely show ill-defined bands, particularly in the case of MM-C138A, where, the bands become mostly negative (Fig. 2C). In addition, MM-C138A exhibits the band at around 292 nm, associable to the L_b transition of the Trp side chain, with the lowest intensity with respect to the other spectra. These features suggest that overall, among the proteins tested, the structure of MM-C138A is more flexible and the Trp19 side chain experiences a higher degree of conformational freedom.

3.2.2. Intrinsic fluorescence spectroscopy

Mus m 1.0102 has a single tryptophan residue (Trp19), key component of the protein core structure (Lücke et al., 1999; Greene et al., 2003, 2001), that provides a unique intrinsic fluorescence probe to detect conformational and environmental modifications. With respect to Mus m 1.0102, where Trp19 fluorescence emission maximum is centred at 339 nm, we detect a red shift of 1 nm for all the mutants (Fig. 2C, *inset*) suggestive of a slightly reduced hydrophobicity of Trp19 environment.

3.2.3. Dynamic light scattering measurements

To evaluate a change in protein conformation and/or the possibility of aggregation, we determined, by DLS, the hydrodynamic size distributions of the proteins.

The volume-weighted size distributions of Mus m 1.0102 and its mutants obtained in native conditions are reported in Fig. 3 (*blue traces)*. The hydrodynamic size distributions of Mus m 1.0102 and MM-C138A display a mean hydrodynamic diameter, calculated according to the Zetasizer μV algorithm, of 3.6 nm and 4.3 nm, respectively; MM-C157A and MM-C138,157A mutants present values of 4.5 nm and 4.4 nm, respectively. The absence of peaks corresponding to larger sizes proves that the presence of aggregates is negligible. The estimates of the protein molecular weight corresponding to the derived hydrodynamic diameters fall in the range 13–22 KDa, which includes the calculated molecular mass of Mus m 1.0102 (18,708 Da) and its mutants. The slight increase of the hydrodynamic diameter of the mutants indicates that the mutations lead to a three dimensional reorganization of the proteins that may contribute, together with other factors, to some of the spectroscopic changes reported by CD and fluorescence spectroscopy (*3.2.1 and 3.2.2 sub-sections*).

3.3. Role of the disulphide bridge on Mus m 1.0102 structure and stability

3.3.1. FTIR spectroscopy

Resolution enhanced infrared spectra (second derivative and deconvoluted) allow the analysis of protein secondary structure: amide I' band (1700–1600 cm^{-1}), mainly arising from the backbone C═O stretching vibration, can be resolved in its component bands characteristic of specific secondary structural elements (Arrondo et al., 1993).

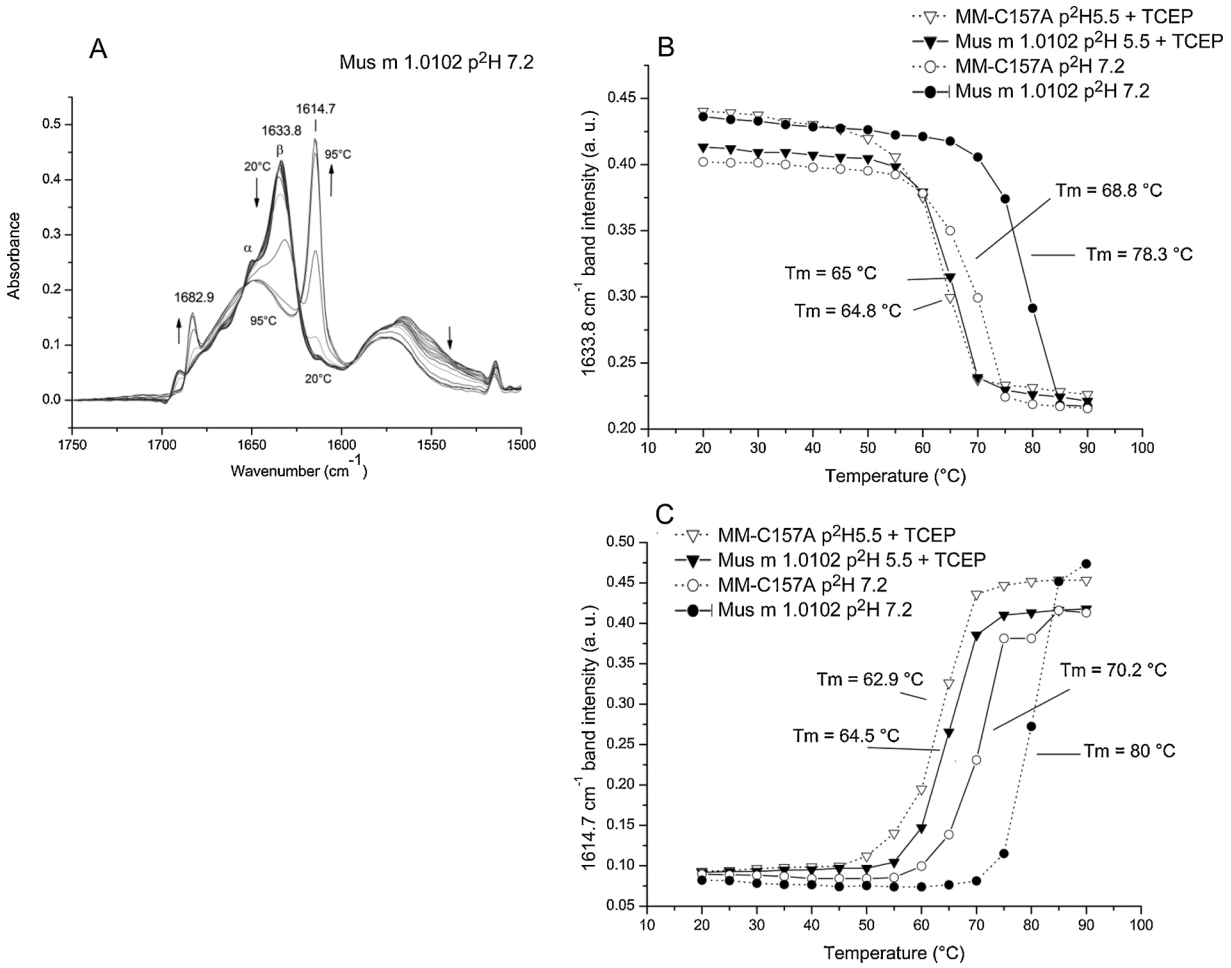

Fig. 5. FTIR analysis of thermal unfolding and aggregation. A. Deconvoluted spectra of Mus m 1.0102 sample at p^2H 7.2, recorded between 20 °C and 95 °C at 5 °C intervals. The arrows (↓) and (↑) indicate the decrease and increase in intensity of the corresponding bands as a function of temperature. B. Intensity of the 1633.8 cm^{-1} β-sheet band, as a function of temperature, for Mus m 1.0102 and MM-C157A, at p^2H 7.2 and at p^2H 5.5 in the presence of 5 mM TCEP. C. Intensity of the 1614.7 cm^{-1} aggregation band as a function of temperature for Mus m 1.0102 and MM-C157A at p^2H 7.2 and at p^2H 5.5 in the presence of 5 mM TCEP.

We examined Mus m 1.0102 and the mutant MM-C157A to disclose how the disulphide bridge affects the protein architecture and thermal stability.

3.3.2. *Proteins secondary structure*

Fig. 4A shows the second derivative spectra of Mus m 1.0102 and MM-C157A acquired at p^2H 7.2. Five bands are detectable in the amide I' region. The 1633.3 and 1691.4 cm^{-1} bands are characteristic of anti-parallel β-sheets, the bands at 1651.1 cm^{-1} and at 1668 cm^{-1} are due to α-helices and turns, respectively, whilst the 1678.5 cm^{-1} band may be due to turns and/or β-sheets. The bands below 1620 cm^{-1} are assigned to amino acid side chain absorptions. In particular, the 1583.1 and 1564.9, cm^{-1} bands are due to the ionized carboxyl groups of aspartic and glutamic acid residues, respectively, and the 1514 cm^{-1} band is characteristic of tyrosine (Barth, 2000).

The spectra do not show significant differences in the intensity and position of the main β-sheet and α-helix bands; only the 1678 cm^{-1} band is a slightly more intense for MM-C157A. Overall, these data indicate that the mutation C157A does not affect appreciably the secondary structure of Mus m 1.0102.

Similarly, the second derivative FTIR spectra of Mus m 1.0102 at p^2H 7.2 and at p^2H 5.5, in the presence of TCEP, do not show significant differences (Fig. 4B), suggesting that the reduction of the disulphide bridge does not affect appreciably the secondary structure of the protein.

Nevertheless, a fine analysis reveals that the spectrum of Mus m 1.0102 obtained at p^2H 5.5, when compared to the one at p^2H 7.2, shows a small increase of the α-helix band intensity, 1651 cm^{-1}, and distinct intensity modifications of the bands at 1583.1 and 1564.9 cm^{-1}, indicative of an alteration of the ionization state of Asp and Glu carboxylic group, respectively. Worth noting that the spectrum recorded at p^2H 5.5, in the presence of TCEP, when compared to the one obtained at neutral p^2H, shows the predictable decrease of glutamic ionization state and an unexpected increase in the ionization state of the aspartic carboxyl group.

An almost similar situation is observed when comparing the spectra of MM-C157A at p^2H 7.2 and at p^2H 5.5, in the presence of TCEP (Fig. 4C). In this case, a slight intensity variation is observed for the 1678.5 cm^{-1} band associated to turns and/or β-sheets, plus a modification of the intensity of the bands at 1583.1 and 1564.9 cm^{-1} similar to the one observed for the wt protein.

Finally, the spectra of Mus m 1.0102 and MM-C157A at p^2H 5.5, in the presence of TCEP, do not reveal significant differences (Fig. 4D), except for the 1678.5 and 1583.8 cm^{-1} bands that are slightly more intense in MM-C157A spectrum.

Taken together, the data of Fig. 4A–D indicate that acidic p^2H, mutation, and reducing conditions slightly affect the protein secondary structure. Furthermore, they suggest that the change in the ionization state of Asp at acidic p^2H is not related to the mutation, but probably to changes in the ionic interactions network induced by the low p^2H.

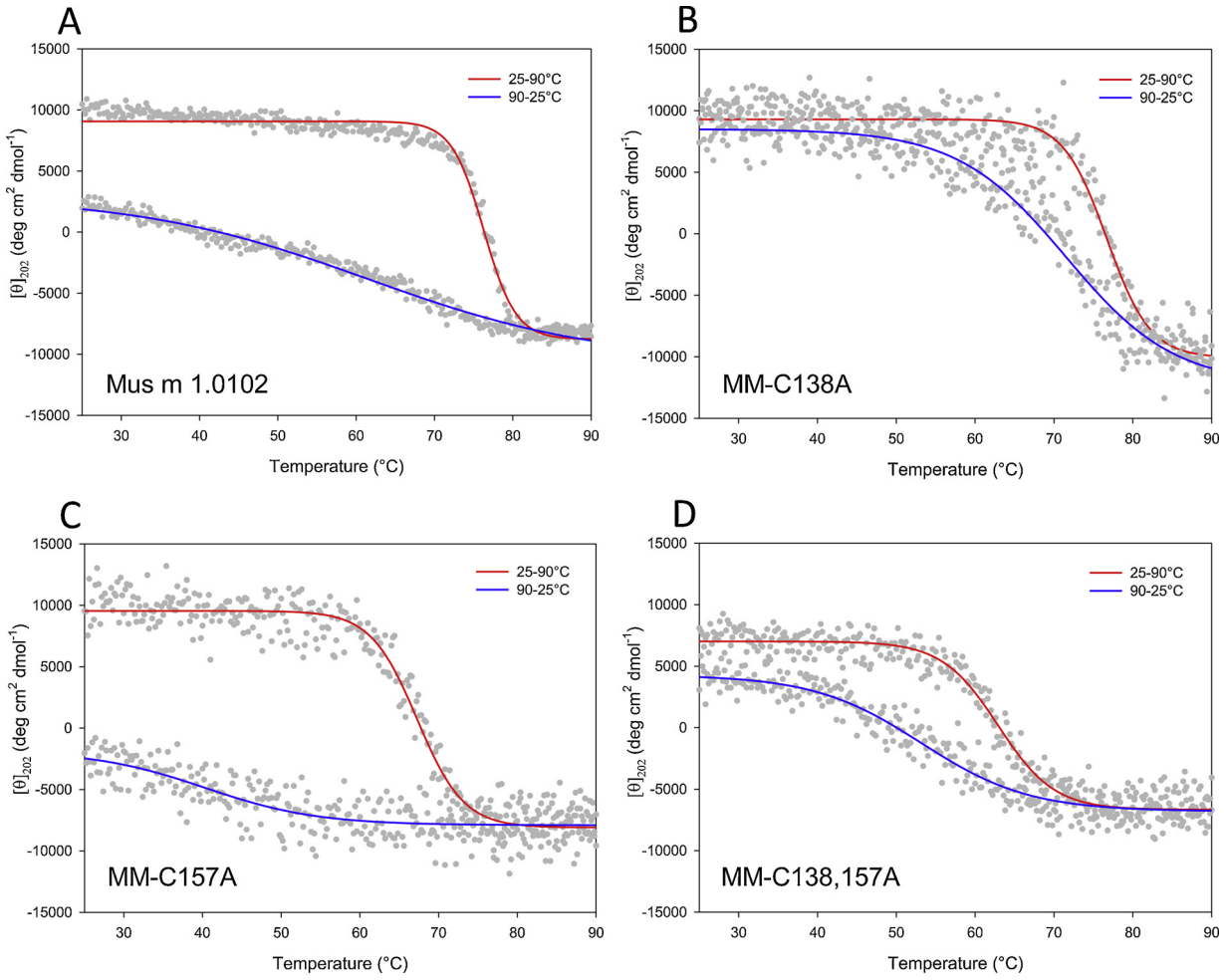

Fig. 6. Thermal unfolding/refolding monitored by CD. The molar ellipticity measured at 202 nm of Mus m 1.0102 and its mutants is presented as a function of temperature (A–D panels). The red transition curves are fitted to the data set recorded during the heating ramp (25 °C–95 °C), while the blue ones are fitted to the data set recorded during the cooling ramp (95 °C-25 °C). Curves equations were used to calculate the following transition midpoints: 76.3 °C and 76.7 °C for the wild type and MM-C138A mutant, respectively, and 67.3 °C and 62.9 °C for MM-C157A and MM-C138,157A mutants, respectively. (For interpretation of the references to colour in this figure legend, the reader is referred to the web version of this article).

3.3.3. Resistance to thermal stress

The intensity of the amide I band (1700–1600 cm^{-1}) is temperature dependent and, according to Scirè (Scirè et al., 2011), it decreases following thermal denaturation of the secondary structure elements. Typically, during thermal denaturation, two new bands close to 1615 and 1680 cm^{-1}, indicative of protein aggregation, can be observed.

Deconvoluted spectra of Mus m 1.0102, recorded at increasing temperatures, are presented in Fig. 5A. Curve fitting of the 1633.8 cm^{-1} (β-sheet) and 1614.7 cm^{-1} (aggregated protein) band intensities clearly highlights the role of the disulphide bridge on protein thermal stability (Fig. 5B and 5C). At p^2H 7.2 the thermal transition midpoint (Tm) of Mus m 1.0102, measured at 1633.8 cm^{-1}, turns out to be about 10 °C higher than for MM-C157A, being 78.3 °C and 68.8 °C, respectively. Differently, at p^2H 5.5, in the presence of TCEP, where both Mus m 1.0102 and MM-C157A do not present the disulphide bridge, their transition midpoint is very similar: 65.0 °C and 64.8 °C, respectively (Fig. 5B).

The T_m of the two proteins, derived from the curves reporting the intensity variation of the 1614.7 cm^{-1} band associated to protein aggregation (Fig. 5C), are just about 2 °C higher than those measured for protein denaturation (Fig. 5B), suggesting that aggregation and denaturation have similar energetics.

It is worth noting that the thermal transition midpoints of denaturation and aggregation for MM-C157A at p^2H 7.2 are higher than those obtained at p^2H 5.5 in the presence of TCEP, indicating that the acidic condition, besides disulphide bridge, affects significantly the stability of the protein.

Protein thermal unfolding was also studied using dynamic light scattering. The temperature data and trends of the light scattering intensity at pH 7.2 are presented in the Data in brief co-submitted article and confirm the IR data on aggregation. Because aggregate formation is revealed by the exponential increase of light scattering intensity, a rough estimate of a T_m can be derived by the trend of the curves: about 70 °C and 60 °C for Mus m 1.0102 and MM-C157A, respectively. The curves, however, provide interesting and reliable indications on the onset of the unfolding process. In fact, data fitting attributes to Mus m 1.0102 and MM-C157A the onset of the unfolding at 62.5 and 52.5 °C, respectively (Tm_{onset}, Table 1), sensibly lower with respect to the temperature at which the proteins secondary elements degrade as revealed by the IR experiments.

Combining the FTIR, DLS and CD data it appears that the disulphide bridge is not directly involved in the preservation of the secondary structure elements. Its absence, however, perturbs the protein intra- and intermolecular ionic interactions leaving the protein more flexible, reducing its resistance to thermal stress and affecting Asp dissociation equilibrium.

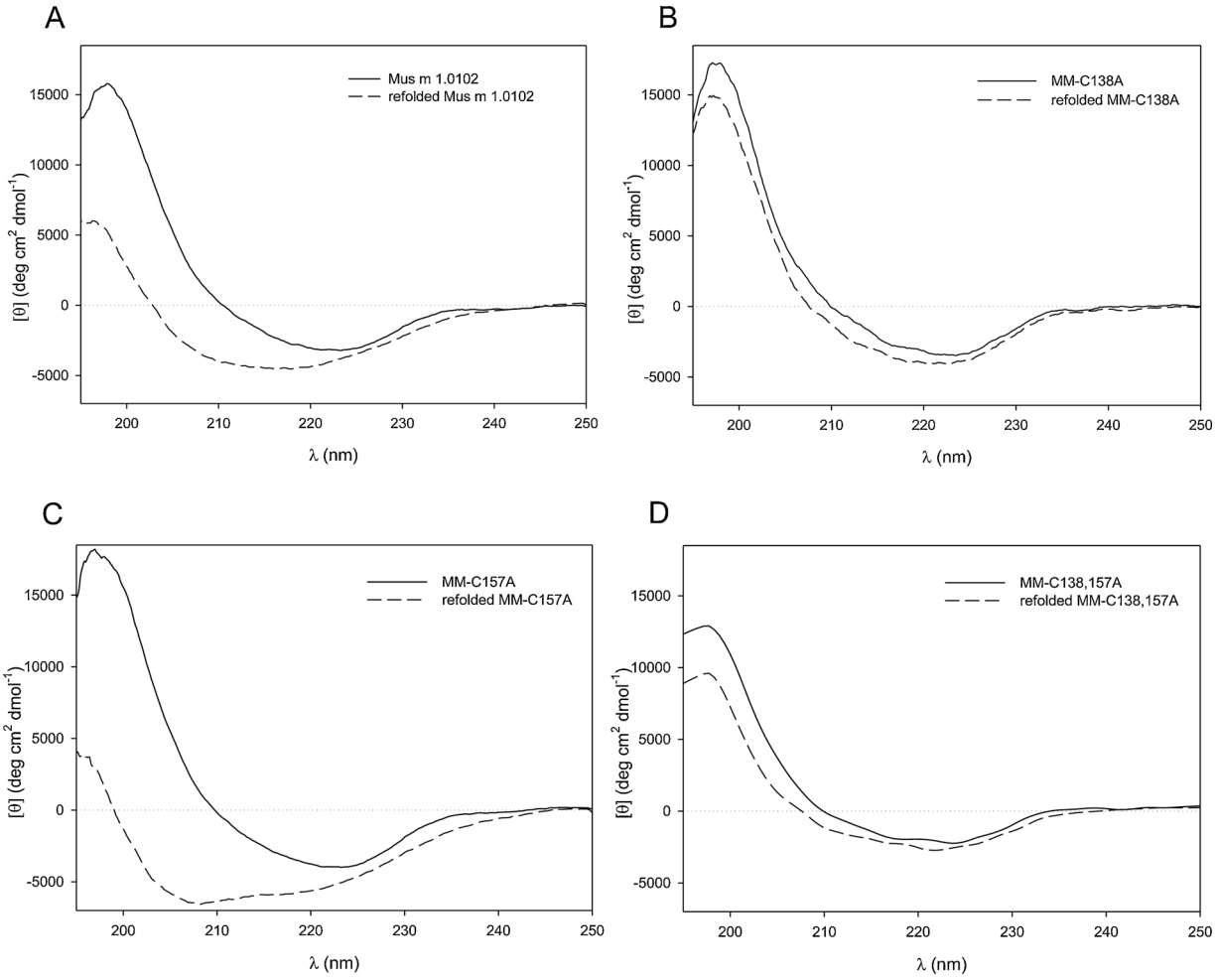

Fig. 7. Reversibility of protein refolding monitored by far-UV CD spectroscopy. Far-UV spectra of Mus m 1.0102 and its mutants (A–D panels): solid line represents the native proteins and the dashed line represents the refolded ones, obtained by gradual cooling after thermal denaturation.

3.4. Reversibility of the thermal unfolding

3.4.1. Circular dichroism spectroscopy

Thermal-induced unfolding and refolding of Mus m 1.0102 and its mutants was investigated by measuring the molar elipticity at 202 nm as a function of temperature, from 25 to 95 °C and then back to 25 °C.

During the unfolding process (Fig. 6, *red fitting curve*), the molar ellipticity decreases for all proteins. The sigmoidal behaviour suggest a biphasic transition. For Mus m 1.0102 and MM-C138A the transition midpoints are 76.3 °C and 76.7 °C, respectively; while for MM-C157A and MM-C138,157A they are 67.3 °C and 62.9 °C, respectively (Tm ± SE, Table 1).

The refolding traces (Fig. 6, *blue fitting curve*), however, highlight a diverse behaviour of the four proteins. In the case of Mus m 1.0102 and MM-C157A, not only the signal at 202 nm does not recover the initial intensity, but also the shape of the refolding curve is completely different, thus suggesting that the proteins do not recover their native fold and that the partial refolding process occurs through a different pathway. In the case of MM-C138A, instead, we observe that the protein conformation returns to an almost native state, travelling through a conformational path similar to the one of the unfolding process. As for MM-C138,157A, it exhibits an intermediate behaviour. It recovers approximately 75 % of the native signal travelling through a conformational path partly similar to the unfolding one.

Fig. 7 compares the far-UV CD spectra of the native samples (*solid lines*) with the correspondent refolded ones (*dashed lines*). Spectra analysis confirms the unfolding irreversibility of both wild-type and MM-C157A mutant, validates the complete recovery of secondary structure elements of the mutant MM-C138A and attributes to the double mutant an intermediate unfolding reversibility.

3.4.2. Intrinsic fluorescence spectroscopy

The maximum emission wavelength (λ_{max}), while increasing the temperature from 25 to 90 °C, highlights a red shift from 339 nm to 354 nm for Mus m 1.0102, from 340 nm to 349 nm for MM-C138A and MM-C157A, from 339 nm to 346 nm for MM-C138,157A (Fig. 8).

The calculated unfolding transition midpoints 78.9 °C and 75.2 °C for MM-C138A and Mus m 1.0102, respectively, indicate an increased resistance of the mutant to heat perturbation; on the contrary, MM-C157A and MM-C138,157A, with transition midpoints of 70.6 °C and 67.4 °C, respectively, exhibit a lower resistance to thermal stress (Tm ± SE, Table 1).

These results are supported by DLS experiments presented in the Data in brief co-submitted article. The data fitting of the temperature trends of the light scattering intensity at pH 7.2 indicate that the onset of the unfolding for MM-C138A is 70.0 °C, higher than the value measured for the native protein, while for MM-C138,157A it is estimated to be 55.0 °C, similar to the one found for MM-C157A (Tm_{onset}, Table 1).

The intrinsic fluorescence emission spectra of the proteins brought back to 25 °C, were compared to the initial ones to evaluate if Trp19 had returned to its local structural microenvironment (Fig. 9). After gradual cooling to 25 °C, Mus m 1.0102 and MM-C157A samples exhibit a λ_{max} of 341 nm and 342 nm, respectively, showing a partial recovery of their original values and a net increase of the total fluorescence

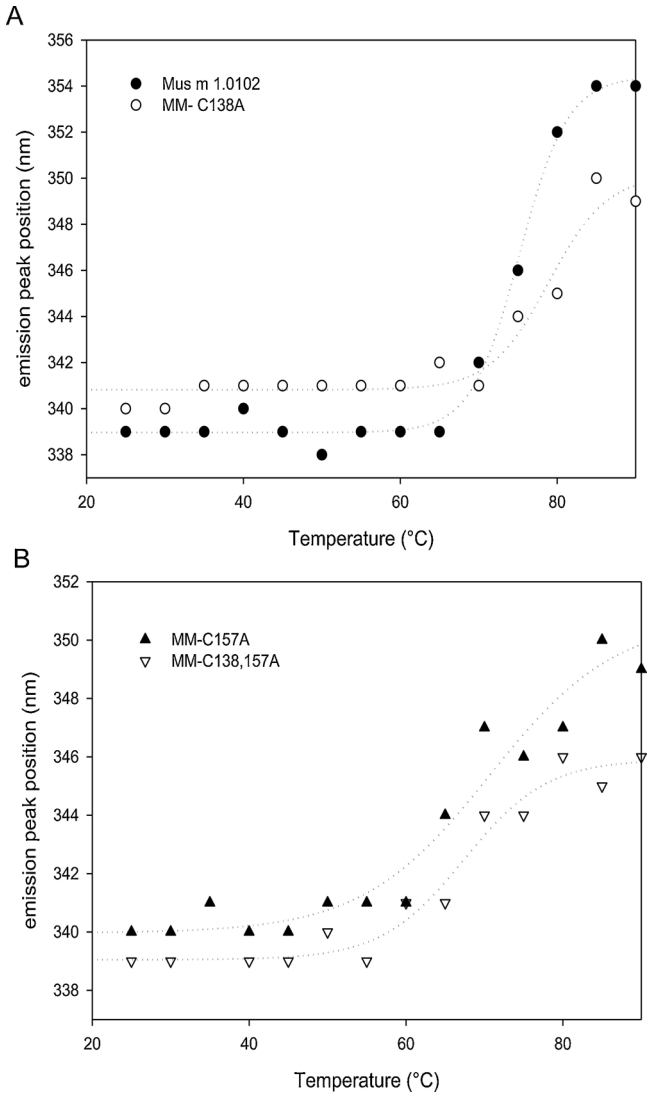

Fig. 8. Thermal unfolding monitored by intrinsic fluorescence. Maximum fluorescence emission wavelength (λ_{max}) of Mus m 1.0102 and its mutants, obtained by exciting at 295 nm, is presented as a function of temperature. A. Equilibrium unfolding data of Mus m 1.0102 and MM-C138A samples. B. Equilibrium unfolding data of MM-C157A and MM-C138,157A mutants. Fitting of the fluorescence data points resulted in the dotted curves whose equations were used to calculate the transition midpoints 75.2 °C and 78.9 °C for Mus m 1.0102 and MM-C138A, respectively; 70.6 °C and 67.4 °C for MM-C157A and MM-C138,157A, respectively.

emission (Fig. 9A and C). This phenomenon is indicative of a non-native environment of the Trp residue. Instead, MM-C138A and MM-C138,157A mutants, both lacking the cysteine residue 138, recover the original fluorescence emission profile (Fig. 9B and D).

3.4.3. Protein size distribution after thermal unfolding and refolding

Evaluation of the molecular size of the proteins cooled down to 25 °C after being heated at 80 °C (*2.4 sub-section* and Data in brief co-submitted article) revealed that Mus m 1.0102, MM-C157A and MM-C138,157A originated size distribution profiles incompatible with the native protein size (Fig. 3, *red traces*), being characterized by macro-aggregates only. Differently, MM-C138A reveals a monomodal size distribution, characterized by a mean hydrodynamic diameter of 4.5 nm, a value comparable with the one of the protein before thermal unfolding (*3.2.3 sub-section*). This finding is consistent with the reversibility of the unfolding process reported by CD and fluorescence spectroscopy, and evidences that C138A substitution contributes to prevent protein aggregation.

3.5. Allergenicity test

The use of passively sensitized RBL cells for comparing allergens potency has been extensively exploited since it represents a good model to generate standardized results (Kaul et al., 2007; Nowak-Wegrzyn et al., 2009). Thus, to assess the allergenicity of the selected proteins, an IgE-mediated degranulation assay was performed using a Rat Basophil Leukemia (RBL) cell line, permanently transfected with the human high-affinity receptor for the Fc region of IgE (FcεRI). The experimental conditions and the data are presented in the Data in brief co-submitted article; a brief description of the results is provided hereafter.

Briefly, to load IgE molecules to the IgE receptors, RBL cells were incubated with sera from nine mouse-allergic individuals and from one control patient sensitized to allergens different from Mus m 1. Subsequently, equimolar amounts of either Mus m 1.0102 or MM-C138A, MM-C157A or MM-C138,157A were added and the extent of FcεRI-dependent degranulation was quantified by measuring the release of β-hexosaminidase.

All proteins reacted with IgE from mouse allergic patients and caused a dose dependent degranulation response. Noteworthy, the degranulation induced by Mus m 1.0102, MM-C138A, MM-C157A or MM-C138,157A revealed a similar quantitative pattern in all tested patients.

No degranulation was induced by challenging the proteins with the cell line that had been treated with serum from the patient who is allergic to cat, dog and horse dander proteins, but not to mouse urine proteins, indicating the Mus m 1-specificity of the test. Stated otherwise, the control patient IgE molecules did not display cross-reactivity to Mus m 1.0102 epitopes, likely due to IgE fine specificity for non-homologous epitopes.

4. Discussion

Today, allergen immunotherapy and allergy diagnostics still depend on allergen extracts, whose efficacy and precision is limited by their heterogeneity and non-perfect formulation reproducibility, thereby affecting the therapeutic and diagnostic management of patients. Recombinant technology provides opportunities for allergen characterization and standardization. Indeed, allergy diagnosis tools have been developed to include specific IgE binding recombinant molecules in monoplex or multiplex format (Matricardi et al., 2016; Ferreira et al., 2014). This approach not only has facilitated the identification of the disease-eliciting molecules and the selection of suitable molecular allergens for specific immunotherapy, but also turned out to be very useful when a specific allergenic component is poorly represented in the natural extract.

Guidelines on the quality of recombinant allergens for immunotherapy as well as allergy diagnostics require a structural characterization of the allergen that, as a prerequisite, must exhibit a reliable conformational stability, a reduced aggregation propensity and an effective IgE-binding ability.

Molecules in solution exist in a dynamic equilibrium among numberless conformations associated to the degree of freedom along their chemical bonds. Particularly in the case of proteins, we can rephrase that issue saying they are in equilibrium among an ensemble of native and partially unfolded microstates. If the equilibrium stochastically favours partially unfolded conformations, then the chances of protein aggregation will increase, driving other folded proteins to aggregation and/or potential degradation. In the opposite situation, we expect that, if we artificially unfold a protein, as soon as the experimental conditions will return to normality the molecular structure will possess enough conformational energy to recover its native status. This complex dynamic process can be associated to the idea of reversible unfolding. When dealing with proteins meant for pharmacological preparations,

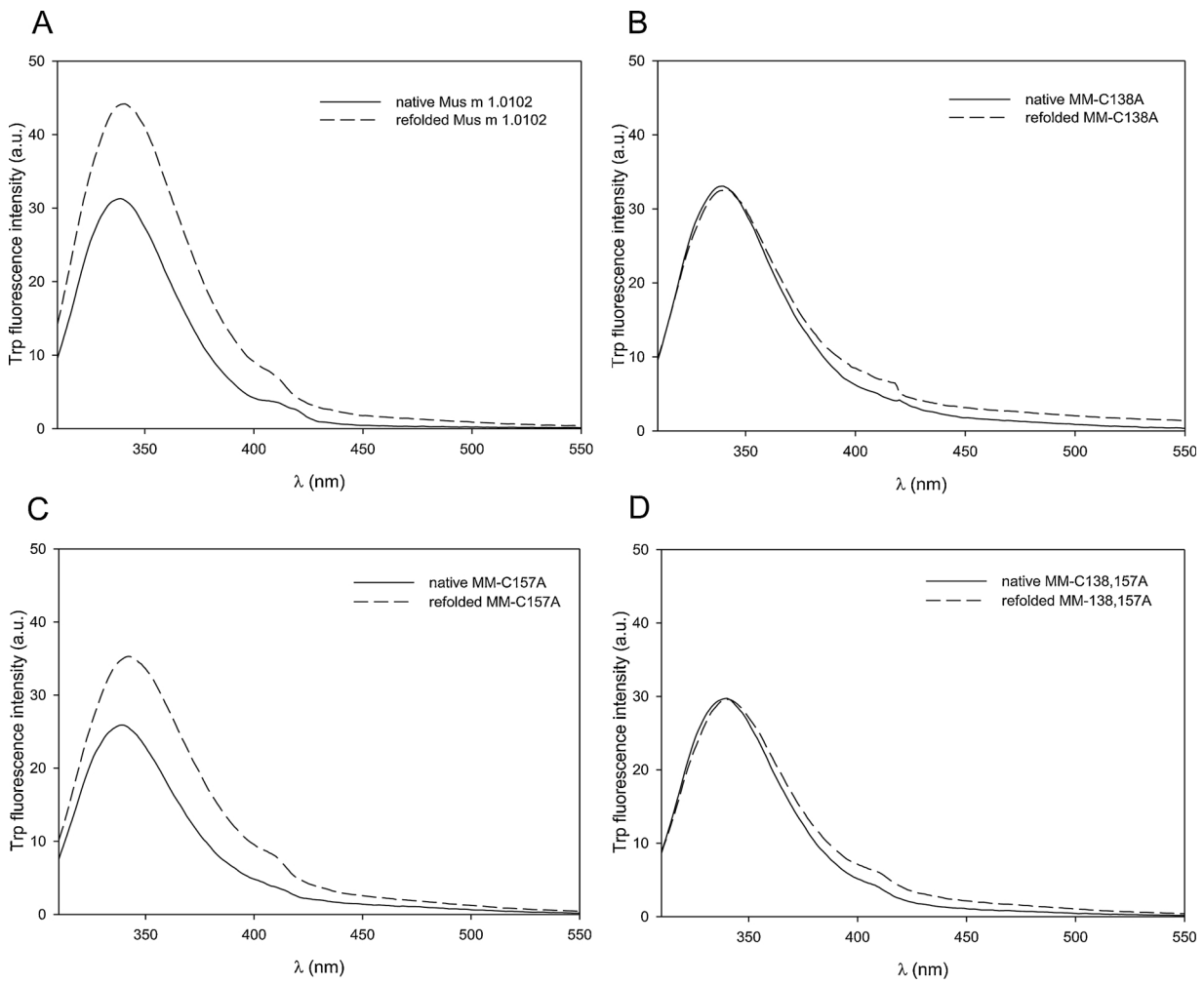

Fig. 9. Reversibility of protein unfolding monitored by intrinsic fluorescence spectroscopy. Tryptophan emission spectra of Mus m 1.0102 and its mutants (A-D panels): solid line represents the native proteins and the dashed line represents the refolded proteins, obtained by gradual cooling. Excitation at 295 nm.

that feature is critical as it assures that, over time, they will preserve their fold and therefore their therapeutic efficacy.

We demonstrated that recombinant Mus m 1.0102 appears inadequate for pharmacological preparations because of its free cysteine in position 138 that, being involved in intra/intermolecular thiol/disulphide exchange, is responsible for a pronounced aggregation propensity (Ferrari et al., 2016). In a first attempt, we designed and characterized the mutant MM-C138S (Ferrari et al., 2016); although monodispersed in solution, it revealed a reduced thermal stability and an enhanced allergenicity, thus turning out to be inadequate for the scope. Those results, however, confirmed the notion that single point mutations produce a complex ensemble of subtle conformational modifications that propagate throughout the molecule affecting, sometimes in unpredictable ways, the protein biological activity (Gagné et al., 2015).

In the present work, the preliminary characterization of the mutants MM-C138A, MM-C157A and MM-C138,157A by western blotting, DLS, CD and Fluorescence spectroscopies, besides an increase of their three dimensional size, as indicated by the relatively larger mean hydrodynamic diameter (*3.2.3 sub-section*), confirmed that they assume a general structural profile comparable with the native protein.

Based on previous experiments demonstrating that only Mus m 1 cavity mutants show a marked difference in the ability to bind NPN (Darwish et al., 2001), we would reasonably expect that the Ala substitution of Cys157 and Cys138 (Fig. 1), mapping outside the hydrophobic pocket, would not drastically influence the affinity for the ligand. Indeed, while this can be appreciated for MM-C138A (Table 1), MM-C138,157A and MM-C157A exhibit a reduced ligand affinity (Table 1). With respect to these last two mutants, it is worth noting that, while mutation of one of the Cys involved in the disulphide bridge leads to a clearly reduced ligand affinity, removal also of the Cys138 narrows the ligand affinity gap with the native protein. Therefore, we can speculate that, in MM-C157A mutant, the presence of the two free thiol groups of Cys64 and Cys138 might increase the ability to generate non-native disulphide bridges as compared to MM-C138,157A mutant. That occurrence is likely to be more effective in perturbing the cavity geometry, thus decreasing MM-C157A ligand binding affinity. As for MM-C138A, interestingly, we may envisage that, the substitution leads to a protein with a slightly more expanded three dimensional size and offers, to the amino acid residues that line the binding pocket, the conformational freedom to acquire a spatial organization more suitable for ligand biding. In addition, the mutant exhibits a reversible unfolding.

Recognizing that the disulphide bond influences lipocalins thermal stability (Ferrari et al., 2016; Pelosi et al., 2014; Liu et al., 2008; Burova et al., 1998), we verified that, for Mus m 1.0102, it contributes to a stabilization of its structure estimated in about 10 °C. It is worth noting that FTIR, CD and Intrinsic Fluorescence show that the destabilizing effect of the secondary and tertiary structure following the substitution C157A, and highlighted by the Tm decrease (*3.3.3 sub-section* and Table 1), is more pronounced with the double substitution C138,157A. This behaviour suggests that, the conformational destabilization induced by the absence of the disulphide bridge is enhanced by the

reduced ability of Ala138 to originate an interaction network as compared to Cys138. The unfolding temperatures (Tm_{onset}, Table 1), are comparably reduced, indicating that the loss of molecular compactness of MM-C157A and MM-C138,157A is equivalent. Conversely, the MM-C138A mutant turns out to be stabilized by the mutation, developing the highest resistance to thermal unfolding.

Overall, the presented results appear to highlight that the presence of the disulphide bridge and the absence of the free cysteine provide the protein with thermal stability, reversibility of unfolding and reduced propensity to aggregate. In a previous work, however, we found that MM-C138S, in spite of the absence of the free cysteine, presents a reduced thermal stability (Ferrari et al., 2016). Taking advantage of the detailed knowledge of the structural architecture of Mus m 1.0102 (Fig. 1) (Lücke et al., 1999; Kuser et al., 2001), we suggest that the tightly packed interface between the α-helix and the β-barrel better accommodates the Ala side chain as compared to the serine or cysteine one (Ferrari et al., 2016). In addition, the Ala side chain hampers the possibility of H-bond formation. These features and their long-range effects on the protein conformation may positively contribute to binding ability, thermal stability and correct refolding, thus limiting aggregation.

As for their allergenicity, the structural similarity of the various mutants justify the comparable dose-dependent degranulation response to the serum IgE of all tested patients. Nonetheless, it is worth noting that MM-C138A does not exhibit the enhanced *in vitro* allergenicity as it was observed for MM-C138S mutant. This is a relevant advancement for its use in immunotherapy and/or diagnostics applications.

5. Conclusions

Indeed fold stability and reversibility of MUPs are the result of a fine combination of various factors that, beside the presence of the disulphide bridge and the free cysteine, are associated also to the physicochemical properties of the amino acid side chains.

We trust these results and the structural and functional features of MM-C138A will turn out to be of interest for researchers in protein science and in the pharmaceutical industry.

The authors ensure that the work described has been carried out in accordance with The Code of Ethics of the World Medical Association (Declaration of Helsinki) for experiments involving humans. Informed consent was obtained for the use of sera from allergic subjects.

CRediT authorship contribution statement

Elena Ferrari: Conceptualization, Investigation, Writing - original draft, Visualization. **Romina Corsini:** Validation, Formal analysis, Investigation. **Samuele E. Burastero:** Investigation, Resources, Writing - original draft. **Fabio Tanfani:** Formal analysis, Investigation, Resources, Writing - original draft. **Alberto Spisni:** Formal analysis, Resources, Writing - review & editing, Supervision, Project administration.

Declaration of Competing Interest

None.

Acknowledgements

We thank the Centro Interdipartimentale Misure “Giuseppe Casnati” of the University of Parma for the use of the CD spectropolarimeter.

This research did not receive any specific grant from funding agencies in the public, commercial, or not-for-profit sectors.

This research has been partly supported by local funds of the University of Parma(FIL 2018-19).

References

Arrondo, J.L., Muga, A., Castresana, J., Goni, F.M., 1993. Quantitative studies of the structure of proteins in solution by Fourier-transform infrared spectroscopy. Prog. Biophys. Mol. Biol. 59, 23–56. https://doi.org/10.1016/0079-6107(93)90006-6.

Ausili, A., Scirè, A., Damiani, E., Zolese, G., Bertoli, E., Tanfani, F., 2005. Temperature-induced molten globule-like state in human α1-Acid glycoprotein: an infrared spectroscopic study. Biochemistry 44, 15997–16006. https://doi.org/10.1021/bi051512z.

Barth, A., 2000. The infrared absorption of amino acid side chains. Prog. Biophys. Mol. Biol. 74, 141–173. https://doi.org/10.1016/S0079-6107(00)00021-3.

Böcskei, Z., Groom, C.R., Flower, D.R., Wright, C.E., Phillips, S.E., Cavaggioni, A., Findlay, J.B., North, A.C., 1992. Pheromone binding to two rodent urinary proteins revealed by X-ray crystallography. Nature 360, 186–188. https://doi.org/10.1038/360186a0.

Burns, J.A., Butler, J.C., Moran, J., Whitesides, G.M., 1991. Selective reduction of disulfides by Tris (2-carboxyethyl) phosphine. J. Org. Chem. 56, 2648–2650. https://doi.org/10.1021/jo00008a014.

Burova, T.V., Choiset, Y., Tran, V., Haertle, T., 1998. Role of free Cys121 in stabilization of bovine β-lactoglobulin. B Protein Eng. 11, 1065–1073. https://doi.org/10.1093/protein/11.11.1065.

Bush, R.K., Stave, G.M., 2003. Laboratory animal allergy: an update. ILAR J. 44, 28–51. https://doi.org/10.1093/ilar.44.1.28.

Canonica, G.W., Ansotegui, I.J., Pawankar, R., Schmid-Grendelmeier, P., van Hage, M., Baena-Cagna ni, C.E., Melioli, G., Nunes, C., Passalacqua, G., Rosenwasser, L., Sampson, H., Sastre, J., Bousquet, J., Zuberbier, T., 2013. AWAO - ARIA - GA2LEN consensus document on molecular-based allergy diagnostics. World Allergy Organ. J. 6, 1–17. https://doi.org/10.1186/1939-4551-6-17.

Cantillo, J., Puerta, L., 2013. From molecular cloning to vaccine development for allergic diseases. An Integrated View of the Molecular Recognition and Toxinology - From Analytical Procedures to Biomedical Applications. Gandhi Rádis Baptista, Brazil. https://doi.org/10.5772/52821. Edited by.

Darwish, M.A., Veggerby, C., Robertson, D.H., Gaskell, S.J., Hubbard, S.J., Martinsen, L., Hurst, J.L., Beynon, R.J., 2001. Effect of polymorphisms on ligand binding by mouse major urinary proteins. Protein Sci. 10, 411–417. https://doi.org/10.1110/ps.31701.

Ferrari, E., Lodi, T., Sorbi, R.T., Tirindelli, R., Cavaggioni, A., Spisni, A., 1997. Expression of a lipocalin in Pichia pastoris: secretion, purification and binding activity of a recombinant mouse major urinary protein. FEBS Lett. 401, 73–77. https://doi.org/10.1016/S0014-5793(96)01436-6.

Ferrari, E., Tsay, A., Eggleston, P.A., Spisni, A., Chapman, M.D., 2004. Environmental detection of mouse allergen by means of immunoassay for recombinant Mus m 1.0102. J. Allergy Clin. Immunol. 114, 341–346. https://doi.org/10.1016/j.jaci.2004.04.028.

Ferrari, E., Breda, D., Longhi, R., Vangelista, L., Nakaie, C.R., Elviri, L., Casali, E., Pertinhez, T.A., Spisni, A., Burastero, S.E., 2012. In search of a vaccine for mouse allergy: significant reduction of Mus m 1.0102 allergenicity by structure-guided single-point mutations. Int. Arch. Allergy Immunol 157, 226–237. https://doi.org/10.1159/000327551.

Ferrari, E., Casali, E., Burastero, S.E., Spisni, A., Pertinhez, T.A., 2016. The allergen Mus m 1.0102: dissecting the relationship between molecular conformation and allergenic potency. Biochim. Biophys. Acta 1864, 1548–1557. https://doi.org/10.1016/j.bbapap.2016.08.003.

Ferreira, F., Wolf, M., Wallner, M., 2014. Molecular approach to allergy diagnosis and therapy. Yonsei Med. J. 55, 839–852. https://doi.org/10.3349/ymj.2014.55.4.839.

Gagné, D., French, R.L., Narayanan, C., Simonović, M., Agarwal, P.K., Doucet, N., 2015. Perturbation of the conformational dynamics of an active-site loop alters enzyme activity. Structure 23, 2256–2266. https://doi.org/10.1016/j.str.2015.10.011.

Greene, L.H., Chrysina, E.D., Irons, L.I., Papageorgiou, A.C., Acharya, K.R., Brew, K., 2001. Role of conserved residues in structure and stability: tryptophans of human serum retinol binding protein, a model for the lipocalin superfamily. Protein Sci. 10, 2301–2316. https://doi.org/10.1110/ps.22901.

Greene, L.H., Hamada, D., Eyles, J.S., Brew, K., 2003. Conserved signature proposed for folding in the lipocalin superfamily. FEBS Lett. 553, 39–44. https://doi.org/10.1016/S0014-5793(03)00925-6.

Hurst, J.L., Payne, C.E., Nevison, C.M., Marie, A.D., Humphries, R.E., Robertson, D.H.L., Cavaggioni, A., Beynon, R.J., 2001. Individual recognition in mice mediated by major urinary proteins. Nature 414, 631–634. https://doi.org/10.1038/414631a.

Jeal, H., Jones, M., 2010. Allergy to rodents: an update. Clin. Exp. Allergy 40 (11), 1593–1601. https://doi.org/10.1111/j.1365-2222.2010.03609.x.

Jutel, M., Agache, I., Bonini, S., Burks, A.W., Calderon, M., Canonica, W., Cox, L., Demoly, P., Frew, A.J., O'Hehir, R., Kleine-Tebbe, J., Muraro, A., Lack, G., Larenas, D., Levin, M., Martin, B.L., Nelson, H., Pawankar, R., Pfaar, O., van Ree, R., Sampson, H., Sublett, J.L., Sugita, K., Du Toit, G., Werfel, T., Gerth van Wijk, R., Zhang, L., Akdis, M., Akdis, C.A., 2015. International consensus on allergy immunotherapy. J. Allergy Clin. Immunol. 136, 556–568. https://doi.org/10.1016/j.jaci.2015.04.047.

Kaul, S., Lüttkopf, D., Kastner, B., Vogel, L., Höltz, G., Vieths, S., Hoffmann, A., 2007. Mediator release assays based on human or murine immunoglobulin E in allergen standardization Clin. Exp. Allergy 37, 141–150. https://doi.org/10.1111/j.1365-2222.2006.02618.x.

Kuser, P.R., Franzoni, L., Ferrari, E., Spisni, A., Polikarpov, I., 2001. The X-ray structure of a recombinant major urinary protein at 1.75 A resolution. A comparative study of X-ray and NMR-derived structures. Acta Crystallogr. D Biol. Crystallogr. 57, 1863–1869. https://doi.org/10.1107/S090744490101825X.

Liu, J., Guo, C., Yao, Y., Lin, D., 2008. Effects of removing a conserved disulfide bond on the biological characteristics of rat lipocalin-type prostaglandin D synthase.

Biochimie 90, 1637–1646. https://doi.org/10.1016/j.biochi.2008.06.003.
Logan, D.W., Marton, T.F., Stowers, L., 2008. Species specificity in major urinary proteins by parallel evolution. PLoS One 3 (9), e3280. https://doi.org/10.1371/journal.pone.0003280.
Lücke, C., Franzoni, L., Abbate, F., Löhr, F., Ferrari, E., Sorbi, R.T., Rüterjans, H., Spisni, A., 1999. Solution structure of a recombinant mouse major urinary protein. Eur. J. Biochem. 266, 1210–1218. https://doi.org/10.1046/j.1432-1327.1999.00984.x.
Matricardi, P.M., Kleine-Tebbe, J., Hoffmann, H.J., Valenta, R., Hilger, C., Hofmaier, S., Aalberse, R.C., Agache, I., Asero, R., Ballmer-Weber, B., Barber, D., Beyer, K., Biedermann, T., Bilo, M.B., Blank, S., Bohle, B., Bosshard, P.P., Breiteneder, H., Brough, H.A., Caraballo, L., Caubet, J.C., Crameri, R., Davies, J.M., Douladiris, N., Ebisawa, M., EIgenmann, P.A., Fernandez-Rivas, M., Ferreira, F., Gadermaier, G., Glatz, M., Hamilton, R.G., Hawranek, T., Hellings, P., Hoffmann-Sommergruber, K., Jakob, T., Jappe, U., Jutel, M., Kamath, S.D., Knol, E.F., Korosec, P., Kuehn, A., Lack, G., Lopata, A.L., Mäkelä, M., Morisset, M., Niederberger, V., Nowak-Wezgrzyn, A.H., Papadopoulos, N.G., Pastorello, E.A., Pauli, G., Platts-Mills, T., Posa, D., Poulsen, L.K., Raulf, M., Sastre, J., Scala, E., Schmid, J.M., Schmid-Grendelmeier, P., van Hage, M., van Ree, R., Vieths, S., Weber, R., Wickman, M., Muraro, A., Ollert, M., 2016. EAACI molecular allergology user's guide pediatr. Allergy Immunol. 27, 1–250. https://doi.org/10.1111/pai.12563.
Matsui, E.C., 2009. Role of mouse allergens in allergic disease. Curr. Allergy Asthma Rep. 9, 370–375. https://doi.org/10.1007/s11882-009-0054-x.
Matsui, E.C., Simons, E., Rand, C., Butz, A., Buckley, T.J., Breysse, P., Eggleston, P.A., 2005. Airborne mouse allergen in the homes of inner-city children with asthma. J. Allergy Clin. Immunol. 115, 358–363. https://doi.org/10.1016/j.jaci.2004.11.007.
Nandy, A., Häfner, D., Klysner, S., 2015. Recombinant allergens in specific immunotherapy: current concepts and developments. Allergo J. Int. 24, 143–151. https://doi.org/10.1007/s40629-015-0054-4.
Nowak-Wegrzyn, A.H., Bencharitiwong, R., Schwarz, J., David, G., Eggleston, P., Gergen, P.J., Liu, A.H., Pongracic, J.A., Sarpong, S., Sampson, H.A., 2009. Mediator release assay for assessment of biological potency of German cockroach allergen extracts. J. Allergy Clin. Immunol. 123, 949–955. https://doi.org/10.1016/j.jaci.2009.01.070.
Pace, C.N., Vajdos, F., Fee, L., Grimsley, G., Gray, T., 1995. How to measure and predict the molar absorption coefficient of a protein. Protein Sci. 4, 2411–2423. https://doi.org/10.1002/pro.5560041120.
Pelosi, P., Mastrogiacomo, R., Iovinella, I., Tuccori, E., Persaud, K.C., 2014. Structure and biotechnological applications of odorant-binding proteins. Appl. Microbiol. Biotechnol. 98, 61–70. https://doi.org/10.1007/s00253-013-5383-y.
Pertinhez, T.A., Ferrari, E., Casali, E., Patel, J.A., Spisni, A., Smith, L.J., 2009. The binding cavity of mouse major urinary protein is optimised for a variety of ligand binding modes. Biochem. Biophys. Res. Commun. 390, 1266–1271. https://doi.org/10.1016/j.bbrc.2009.10.133.
Phelan, M.M., McLean, L., Armstrong, S.D., Hurst, J.L., Beynon, R.J., Lian, L.Y., 2014. The structure, stability and pheromone binding of the male mouse protein sex pheromone darcin. PLoS One 9, e108415. https://doi.org/10.1371/journal.pone.0108415.
Ricatti, J., Acquasaliente, L., Ribaudo, G., De Filippis, V., Bellini, M., Llovera, R.E., Barollo, S., Pezzani, R., Zagotto, G., Persaud, K.C., Mucignat-Caretta, C., 2019. Effects of point mutations in the binding pocket of the mouse major urinary protein MUP20 on ligand affinity and specificity. Sci. Rep. 9, 300. https://doi.org/10.1038/s41598-018-36391-3.
Roberts, S.A., Prescott, M.C., Davidson, A.J., McLean, L., Beynon, R.J., Hurst, J.L., 2018. Individual odour signatures that mice learn are shaped by involatile major urinary proteins (MUPs). BMC Biol. 16, 48. https://doi.org/10.1186/s12915-018-0512-9.
Salomaa, P., Schaleger, L.L., Long, F.A., 1964. Solvent deuterium isotope effects on acid-base equilibria. J. Am. Chem. Soc. 86, 1–7. https://doi.org/10.1021/ja01055a001.
Sartor, G., Pagani, R., Ferrari, E., Sorbi, R.T., Cavaggioni, A., Cavatorta, P., Spisni, A., 2001. Determining the binding capability of the mouse major urinary proteins using 2-naphthol as a fluorescent probe. Anal. Biochem. 292, 69–75. https://doi.org/10.1006/abio.2001.5065.
Sastre, J., 2010. Molecular diagnosis in allergy. Clin. Exp. Allergy 40, 1442–1460. https://doi.org/10.1111/j.1365-2222.2010.03585.x.
Scirè, A., Baldassarre, M., Lupidi, G., Tanfani, F., 2011. Importance of pH and disulfide bridges on the structural and binding properties of human α1-acid glycoprotein. Biochimie 93, 1529–1536. https://doi.org/10.1016/j.biochi.2011.05.008.
Sharrow, S.D., Edmonds, K.A., Goodman, M.A., Novotny, M.V., Stone, M.J., 2005. Thermodynamic consequences of disrupting a water-mediated hydrogen bond network in a protein:pheromone complex. Protein Sci. 14, 249–256. https://doi.org/10.1110/ps.04912605.
Stetefeld, J., McKenna, S.A., Patel, T.R., 2016. Dynamic light scattering: a practical guide and applications in biomedical sciences. Biophys. Rev. 8, 409–427. https://doi.org/10.1007/s12551-016-0218-6.
Timm, D.E., Baker, L.J., Mueller, H., Zidek, L., Novotny, M.V., 2001. Structural basis of pheromone binding to mouse major urinary protein (MUP-I). Protein Sci. 10, 997–1004. https://doi.org/10.1110/ps.52201.
Tirindelli, R., Dibattista, M., Pifferi, S., Menini, A., 2009. From pheromones to behavior. Physiol. Rev. 89, 921–956. https://doi.org/10.1152/physrev.00037.2008.
Tscheppe, A., Breiteneder, H., 2017. Recombinant allergens in structural biology, diagnosis, and immunotherapy. Int. Arch. Allergy Immunol. 172, 187–202. https://doi.org/10.1159/000464104.
Wintersand, A., Asplund, K., Binnmyr, J., Holmgren, E., Nilsson, O.B., Gafvelin, G., Grönlund, H., 2019. Allergens in dog extracts: implication for diagnosis and treatment. Allergy 74, 1472–1479. https://doi.org/10.1111/all.13785.
Xia, X., Longo, L.M., Blaber, M., 2015. Mutation choice to eliminate buried free cysteines in protein therapeutics. J. Pharm. Sci. 104, 566–576. https://doi.org/10.1002/jps.24188.
Zahradnik, E., Raulf, M., 2014. Animal allergens and their presence in the environment. Front. Immunol. 5, 76. https://doi.org/10.3389/fimmu.2014.00076.